

Influence of alkali-fluoride insertion layers on the perpendicular magnetic anisotropy at the Fe/MgO interface

Jieyi Chen ¹, Shoya Sakamoto ^{1,*} and Shinji Miwa ^{1,2,†}

¹The Institute for Solid State Physics, The University of Tokyo, Chiba 277-8581, Japan

²Trans-Scale Quantum Science Institute, The University of Tokyo, Tokyo 113-0033, Japan



(Received 30 November 2023; accepted 24 January 2024; published 15 February 2024)

The Fe/MgO interface is a cornerstone of spintronics applications, where enhancing its perpendicular magnetic anisotropy (PMA) has been a formidable challenge. Recent studies have reported an increase in PMA by introducing an ultrathin LiF layer, hinting at the potential of fluorine atoms with strong electronegativity. However, the underlying cause of this enhancement, whether stemming from the strong electronegativity of fluorine atoms or improved lattice matching, remains uncertain. In this paper, to disentangle these two contributing factors, we introduce a NaF layer with suboptimal lattice matching at the Fe/MgO interface and investigate the magnetic anisotropy energy. We find that the interfacial PMA energy is enhanced by the insertion of a 0.1-nm-thick NaF layer but weakened by a thicker NaF layer insertion (0.2–1 nm). The observed PMA enhancement, even in an Fe/NaF interface with suboptimal lattice matching, highlights the essential role of Fe-F orbital hybridization. Our findings shall provide a foundational basis for dielectric layer design to strengthen the PMA of ultrathin ferromagnetic layers.

DOI: [10.1103/PhysRevB.109.064413](https://doi.org/10.1103/PhysRevB.109.064413)

I. INTRODUCTION

Magnetoresistive random access memory, consisting of magnetic tunnel junctions (MTJs), is a promising next-generation nonvolatile memory. In an MTJ, binary information is encoded as either parallel or antiparallel magnetization directions in two ferromagnetic layers separated by an insulating barrier layer. Fe/MgO-based systems have attracted significant attention because of their strong perpendicular magnetic anisotropy (PMA) [1–4] and giant tunneling magnetoresistance (TMR) [5,6]. Numerous studies attempted to improve PMA energy to guarantee a long information retention time by optimizing the MTJ structure. This optimization includes modifying the epitaxial strain through the annealing process [2,7] or strengthening the spin-orbit coupling by introducing heavy metal elements into the Fe layers [8–11]. The significance of lattice matching has also been investigated, as better lattice matching may result in fewer interfacial defects and higher epitaxial quality. For instance, earlier studies employed a spinel oxide MgAl₂O₄ barrier with excellent lattice matching to Fe (<1%) and demonstrated a comparable MR ratio and interfacial PMA with those of Fe/MgO [12–16]. Recently, it was reported that an ultrathin LiF layer insertion at the Fe/MgO interface can enhance the interfacial PMA while maintaining the TMR ratio [17,18], and a following study showed that inserting other alkali-halide layers, such as NaCl and CsI, degrades the interfacial PMA [19]. Such findings suggest the importance of the strong electronegativity of fluorine atoms (F⁻ > O²⁻). However, given that LiF has

better lattice matching with Fe than MgO does ($a_{\text{LiF}} = 4.03 \text{ \AA}$, $a_{\text{MgO}} = 4.21 \text{ \AA}$, $\sqrt{2}a_{\text{Fe}} = 4.05 \text{ \AA}$), it remains unclear whether the presence of fluorine atoms on the Fe atoms or the improved lattice matching between Fe and LiF layers contributes more significantly to the PMA enhancement.

In this paper, in order to disentangle the effects of strong electronegativity and lattice matching, we insert an ultrathin NaF layer with suboptimal lattice matching to Fe at the Fe/MgO interface and characterize the PMA energy. NaF, LiF, and MgO share the same NaCl-type crystal structure with lattice constants of 4.62, 4.03, and 4.21 Å, respectively [20], and grow epitaxially on Fe with a lattice constant of $\sqrt{2}a_{\text{Fe}} = 4.05 \text{ \AA}$. We find that the insertion of a 0.1-nm-thick NaF layer enhances the interfacial PMA while retaining the bulk anisotropy. This indicates that the PMA enhancement through Fe-F hybridization counters the PMA degradation resulting from interfacial defects due to lattice mismatch, highlighting the importance of Fe-F orbital hybridization.

II. EXPERIMENT

The schematic of the multilayer structure is shown in Fig. 1(a). The multilayers consist of single-crystalline MgO (001) substrate/MgO (5 nm)/V (30 nm)/Fe ($t_{\text{Fe}} = 0.3\text{--}0.9 \text{ nm}$)/NaF (0–1 nm)/MgO (5 nm)/SiO₂ (5 nm) and were fabricated by molecular beam epitaxy in an ultrahigh-vacuum environment. The V underlayer was employed because as-deposited V/Fe/MgO multilayers show large PMA without requiring a post-annealing process [7,21]. Preceding the deposition, the MgO substrate underwent annealing at 800 °C for 10 min to obtain a clean surface, followed by the growth of a 5-nm-thick MgO layer at a rate of 0.1 Å/s to prevent carbon impurity diffusion from the substrate into the metal layers.

*shoya.sakamoto@issp.u-tokyo.ac.jp

†miwa@issp.u-tokyo.ac.jp

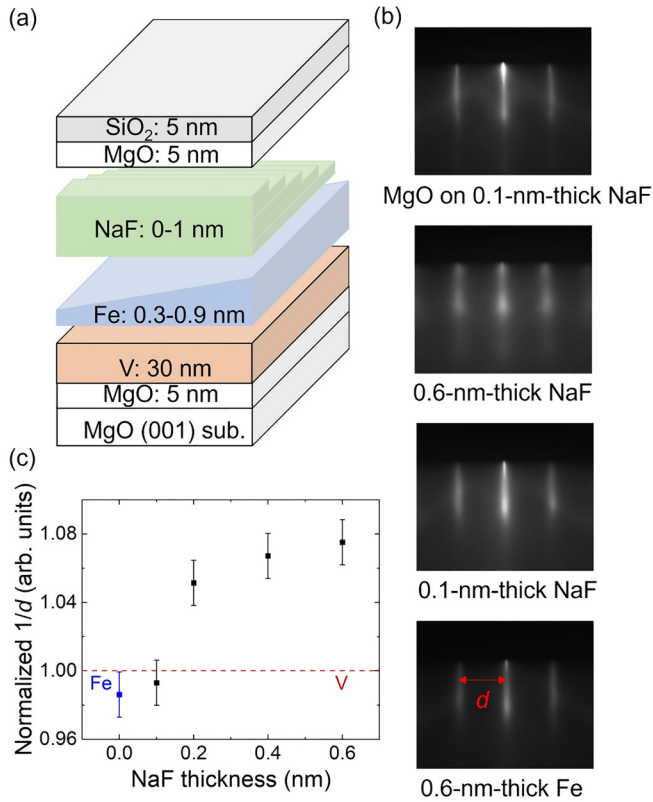


FIG. 1. (a) Schematic of the multilayers. (b) RHEED patterns of the multilayers: 0.6-nm-thick Fe layer, 0.1- and 0.6-nm-thick NaF layers, and MgO overlayer on 0.1-nm-thick NaF layer. All the RHEED patterns are screened along the MgO [100] zone axis. (c) Normalized reciprocal of the distance between streaks ($1/d$) in V, Fe, and NaF epilayers obtained from pixel analysis. Here the V layer is chosen as a reference and denoted as a red dashed line. The 0-nm-thick NaF layer is denoted as a blue point, corresponding to the Fe underlayer.

Subsequently, a 30-nm-thick V layer was deposited at a rate of $\sim 0.15 \text{ \AA/s}$ and annealed at 500°C for 20 min to ensure a smooth surface. The Fe and NaF layers were grown at a slower rate of $\sim 0.05 \text{ \AA/s}$ to precisely control their thickness. A 5-nm-thick MgO cap layer was then grown on the NaF layer at a rate of $\sim 0.1 \text{ \AA/s}$. For surface protection, a 5-nm-thick SiO_2 layer was deposited using the sputtering method. Surface crystallinity was assessed via reflection high-energy electron diffraction (RHEED) measurements. Magnetic properties were characterized by conducting polar magneto-optical Kerr effect (polar-MOKE) measurements at room temperature. Visible light with a 660-nm wavelength was perpendicularly impinging on the sample surface, and perpendicular magnetic fields of up to 1.3 T were applied.

III. RESULTS AND DISCUSSION

We performed RHEED measurements to examine the crystallinity of the NaF layers. The RHEED images of the 0.6-nm-thick Fe layer, 0.1- and 0.6-nm-thick NaF layers, and the corresponding MgO cap layer on the 0.1-nm-thick NaF layer, are shown in Fig. 1(b), respectively. The sharp streaks observed in the RHEED pattern of the Fe layer signify an

atomically flat, single-crystalline surface. The streaky patterns observed in the RHEED images of the 0.1- and 0.6-nm-thick NaF layers indicate the epitaxial growth of the NaF layer on the Fe layer. The RHEED pattern of the MgO overlayer on the 0.1-nm-thick NaF layer also shows a sharp streaky pattern, indicating the well-epitaxial deposition of the MgO layer on the ultrathin NaF layer. This suggests a potential of the Fe/NaF/MgO trilayer as a dielectric layer for MTJ application, as in the case of the Fe/LiF/MgO structure [17].

To evaluate the lattice matching properties, we estimated the in-plane lattice constants of the NaF layers with various thicknesses by measuring the distance between the streaks in the RHEED patterns [represented as d in Fig. 1(b)]. As the in-plane lattice constant is inversely proportional to d , we plotted $1/d$ values for the Fe and NaF layers normalized to that for the V layer in Fig. 1(c). The in-plane lattice constant of the reference V layer is indicated by a red dashed line, while the lattice constant of the Fe underlayer is plotted in blue at a NaF thickness of 0 nm. Error bars in the plot represent one pixel of the images. Shifting the electron beam on the sample surface to different regions with various NaF thicknesses did not significantly alter the d values, as verified by changing the beam position on the uniform V layer. Assuming that the in-plane lattice constant of the V layer is the same as the bulk lattice constant ($a_V = 3.03 \text{ \AA}$), neglecting its slight compression ($<1\%$) induced by the epitaxial strain from the MgO substrate [7], the in-plane lattice constant of the Fe layer is evaluated as $\sim 2.99 \text{ \AA}$. This lattice constant value matches well with that of the MgO layer ($a_{\text{MgO}}/\sqrt{2} = 2.98 \text{ \AA}$).

Regarding the NaF layers, the $1/d$ value remained constant with a 0.1-nm-thick NaF insertion but drastically increased when the NaF thickness exceeded 0.1 nm. The in-plane lattice constant of the 0.6-nm-thick NaF layer is estimated as $\sim 3.23 \text{ \AA}$, approaching its unconstrained bulk lattice constant ($a_{\text{NaF}}/\sqrt{2} = 3.27 \text{ \AA}$). These results indicate that a NaF layer epitaxially forms islands on the Fe layer when the NaF layer is thinner than a monolayer. However, for thicker NaF layer insertions, accumulated internal stress overcomes the epitaxial stress and creates interfacial defects, and therefore, the lattice constant approaches the bulk lattice constant. On the other hand, an LiF layer can grow epitaxially without forming interfacial defects up to a larger thickness of 0.4 nm due to its superior lattice matching [19].

The Fe thickness dependence of polar-MOKE hysteresis loops for the sample with a 0.1-nm-thick NaF layer is shown in Fig. 2(a). Squarelike hysteresis loops confirm the presence of PMA. Figure 2(b) shows the Fe thickness dependence of saturated Kerr rotation angles obtained from the PMA magnetization curves for various NaF thicknesses. The penetration depth ($\sim 17 \text{ nm}$) of incident 660 nm light [22] is much longer than the Fe thicknesses, allowing the Kerr rotation angle to be proportional to the Fe magnetization and thickness. This relationship can be expressed as $\alpha M_{\text{eff}}(t_{\text{Fe}} - t_{\text{DL}})$, where α is the proportionality constant, M_{eff} represents the effective magnetization or magnetization in the bulk region, t_{Fe} is the nominal Fe thickness, and t_{DL} represents the thickness of a magnetically dead layer near the interface. The proportionality constant α is determined by our previous x-ray magnetic circular dichroism measurements, where an average magnetic moment of $2.17 \mu_B/\text{Fe}$ was deduced for the V/Fe

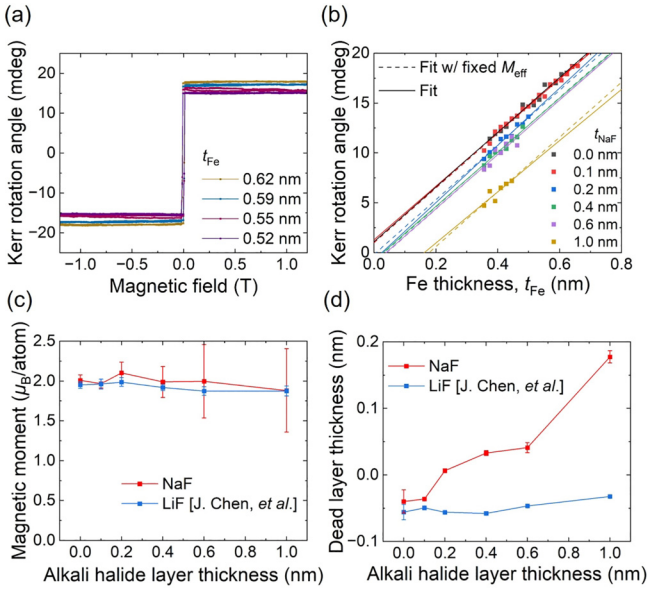


FIG. 2. (a) Hysteresis loops of the NaF 0.1-nm samples with various Fe thicknesses measured using the polar magneto-optic Kerr effect. (b) Fe thickness dependence of the saturation Kerr rotation angle. NaF and LiF (Ref. [19]) thickness dependence of the (c) magnetic moment and the (d) dead layer. Reprinted LiF data with permission from [19].

(0.5 nm)/MgO multilayer [7]. We assume that the proportionality constant does not change for different NaF thicknesses.

Saturation Kerr rotation angle data are fitted to estimate the effective magnetization and the dead layer thickness. The solid lines in Fig. 2(b) represent the fit with both magnetization and dead layer thickness as free parameters. The obtained magnetization values of the NaF sample and the control LiF sample [19] are plotted in Fig. 2(c). Similar to the LiF case, the magnetization of the NaF sample remains unchanged within error bars. Consequently, we used the effective magnetization of the Fe/MgO for the NaF-inserted regions for further analysis. The results of such fixed-magnetization (fixed-slope) fitting are depicted by dashed lines in Fig. 2(b). The overlap between the solid and dashed lines again suggests that the bulk magnetization is unaffected by NaF insertion. The magnetic dead layer thickness of the NaF sample and the compared LiF sample obtained by the fixed-magnetization fit is shown in Fig. 2(d). A near-zero but negative dead layer thickness at the Fe/MgO interface without LiF or NaF insertion indicates the interfacial enhancement of the magnetic moment [23]. The dead layer exhibits robustness after LiF insertion and remains unchanged with a 0.1-nm-thick NaF insertion. However, it drastically increases as the NaF thickness becomes thicker, suggesting interlayer mixing between NaF and Fe layers.

The Fe thickness dependence of normalized polar-MOKE hysteresis loops for Fe/MgO and Fe/NaF (0.1 nm)/MgO are shown in Figs. 3(a) and 3(b), respectively. Linear background subtraction was applied to all the data. As in-plane shape magnetic anisotropy becomes dominant with increasing Fe thickness, the magnetic anisotropy transforms from perpendicular to in plane at a certain Fe thickness. This transformation is evident in the change of the hysteresis loop from a squarelike shape with a sudden jump near zero mag-

netic field [see the black curves in Figs. 3(a) and 3(b)] to a more rounded shape with gradual increase as a function of magnetic fields [see the red and green curves in Figs. 3(a) and 3(b)]. The robustness of magnetization against the perpendicular magnetic field manifests the strength of in-plane magnetic anisotropy. The Fe/MgO exhibits larger in-plane magnetic anisotropy than the Fe/NaF (0.1 nm)/MgO, indicating that the 0.1-nm-thick NaF insertion increases interfacial PMA.

The PMA energy K_{eff} represents the magnetic energy difference under in-plane and out-of-plane magnetic fields and is given by [24]

$$K_{eff} = \mu_0 M_{eff} \left\{ \int_0^1 H_{IP} d\hat{M}_{IP} - \int_0^1 H_{OP} d\hat{M}_{OP} \right\}, \quad (1)$$

where M_{eff} represents the effective saturation magnetization deduced above. H_{IP} (H_{OP}) and \hat{M}_{IP} (\hat{M}_{OP}) denote the in-plane (out-of-plane) magnetic field and corresponding magnetization normalized by saturation magnetization, respectively. This expression corresponds to the work needed to align magnetization from the in-plane to the out-of-plane direction. Each term can be calculated as an area between each normalized magnetization curve and the magnetization axis [see the shaded area in the inset of Fig. 3(b), for example]. In the present system, the easy-axis magnetization curves are square, and therefore, we ignored the first term for magnetic anisotropy energy estimation.

Here we decompose the contribution from the interfacial (K_I) and bulk (K_V) magnetic anisotropy to the PMA energy using the following expression [25]:

$$K_{eff} t_{eff} = (K_V - \frac{1}{2} \mu_0 M_{eff}^2) t_{eff} + K_I. \quad (2)$$

The effective Fe thickness t_{eff} is defined as the nominal Fe thickness subtracted by the dead layer thickness, and the shape magnetic anisotropy is included as the second term in the parentheses. $K_{eff} t_{eff}$ values as a function of t_{eff} are plotted in Fig. 3(c), where the positive and negative values represent perpendicular and in-plane magnetic anisotropy energies. K_I and K_V are deduced as the y intercept and the slope of the linear fit from Eq. (1). The results of the NaF sample and the LiF sample [19] are shown in Figs. 3(d) and 3(e), respectively. For the NaF sample, K_I and K_V are estimated as $K_I \sim 2 \text{ mJ/m}^2$ and $K_V \sim -1 \text{ MJ/m}^3$ in the Fe/MgO region. These values are consistent with those reported in a previous study, ensuring the sample quality [19].

The 0.1-nm-thick NaF insertion shows a slight enhancement of K_I while maintaining the K_V value. For the thicker NaF insertion, both K_I and K_V weaken with the increasing NaF thickness. Such behavior is similar to the LiF case, except that K_I and K_V weakening occurs at a larger LiF thickness of 0.4 nm [19]. This critical thickness difference between Fe/LiF and Fe/NaF probably originates from the difference in lattice matching conditions. The weakening of K_I probably originates from interface dislocations created upon releasing accumulated internal stress and from an intermixing of the NaF and Fe layers, as discussed above. In fact, the increase of magnetic dead layers [Fig. 2(d)] strongly suggests the increase of intermixing at the Fe/NaF interface [26–28]. The interlayer mixing can also be a reason for the weakening of interfacial PMA and bulk in-plane magnetocrystalline anisotropy.

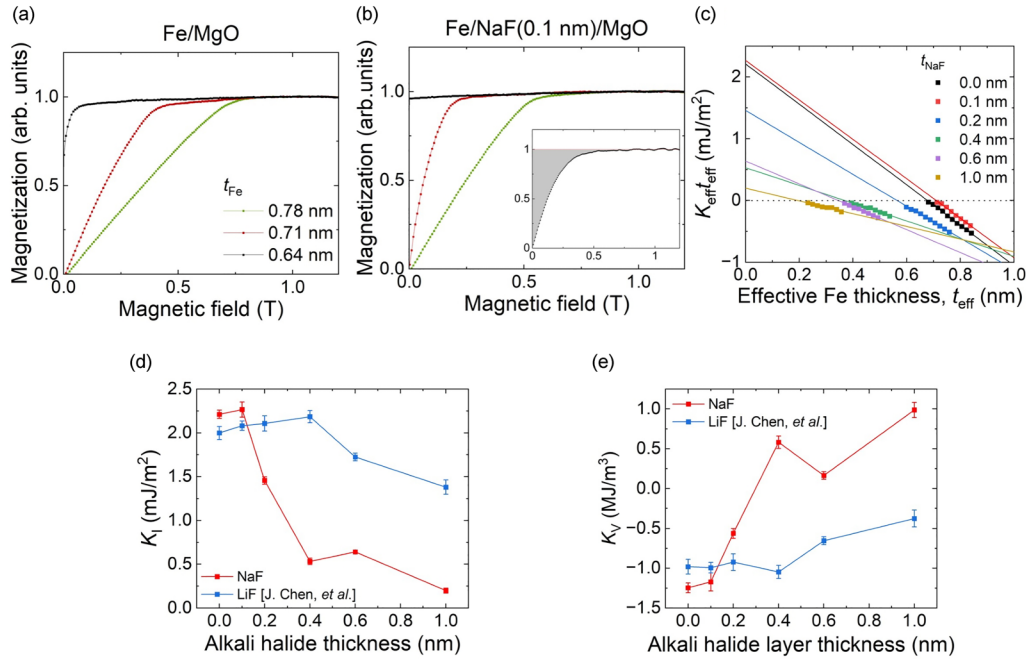


FIG. 3. Normalized magnetization curves for the (a) Fe/MgO and (b) with 0.1-nm-thick NaF layer insertion. The magnetic anisotropy energies K_{eff} are estimated from the magnetization curves, as indicated in the shaded area in the inset in (b). (c) Magnetic anisotropy energy multiplied by the effective Fe thickness $K_{\text{eff}}t_{\text{eff}}$ as a function of the effective Fe thickness. (d) Interfacial (K_I) and (e) volume (K_V) magnetic anisotropy energies as a function of NaF and LiF thickness. Reprinted LiF data with permission from [19].

Finally, let us discuss the origin of the K_I enhancement. Previous studies on interfacial magnetic anisotropy at the Fe/LiF interface attributed the origin of the K_I enhancement to either the strong electron negativity of fluorine atoms or the improved lattice matching [17–19]. The present results, which demonstrated K_I enhancement in the Fe/NaF interface despite suboptimal lattice matching, underscore the importance of fluorine atoms on the Fe atoms. We infer that the stronger ionic nature of LiF and NaF compared to MgO modifies the interfacial electronic structure and results in more robust electron localization at the interface. Such electron localization strengthens electron-electron correlation and enhances PMA energies [18]. A previous theoretical study pointed out the importance of interstitial fluorine or oxygen impurities located within the topmost Fe layer and suggested that the reduction of PMA energy caused by interstitial F atoms is not as significant as that caused by interstitial oxygen atoms [29]. Nevertheless, Fe oxidation due to interstitial oxygen atoms in the Fe layer might not be significant [30], and a deeper microscopic understanding of PMA enhancement by fluoride layer insertion may still be necessary.

IV. CONCLUSION

In this study, we have investigated the influence of NaF insertion on magnetic anisotropy at the Fe/MgO interface

to disentangle the effects of fluorine electron negativity and lattice matching. The insertion of a 0.1-nm-thick NaF layer enhanced interfacial PMA while retaining bulk magnetic anisotropy. Insertion of a thicker NaF layer weakened both interfacial PMA and bulk magnetic anisotropy. This reduction was attributed to interface dislocation and interlayer mixing. The enhancement in interfacial PMA caused by the insertion of an ultrathin NaF layer with relatively unmatched lattice constants underscores the significance of having fluorine atoms on the Fe atoms and their orbital hybridization. These findings deepen our understanding of magnetic anisotropy at the Fe/MgO interface influenced by fluoride insertion, offering valuable insights for the continued advancement of magnetic tunnel junction structures for memory applications.

ACKNOWLEDGMENTS

We thank T. Higo and S. Nakatsuji of the University of Tokyo for MOKE measurements. This work was partly supported by JSPS KAKENHI (Grants No. JP22H00290, No. JP22H04964, No. JP22K18320, and No. JP23H01833), the Spintronics Research Network of Japan (Spin-RNJ), JST-Mirai Program (JPMJMI20A1), and MEXT Initiative to Establish Next-Generation Novel Integrated Circuit Centers (X-NICS; Grant No. JPJ011438).

[1] S. Yakata, H. Kubota, Y. Suzuki, K. Yakushiji, S. Yuasa, and K. Ando, *J. Appl. Phys.* **105**, 07D131 (2009).

[2] S. Ikeda, K. Miura, H. Yamamoto, K. Mizunuma, H. D. Gan, M. Endo, S. Kanai, J. Hayakawa, F. Matsukura, and H. Ohno, *Nat. Mater.* **9**, 721 (2010).

- [3] H. X. Yang, M. Chshiev, B. Dieny, J. H. Lee, A. Manchon, and K. H. Shin, *Phys. Rev. B* **84**, 054401 (2011).
- [4] C.-H. Lambert, A. Rajanikanth, T. Hauet, S. Mangin, E. E. Fullerton, and S. Andrieu, *Appl. Phys. Lett.* **102**, 122410 (2013).
- [5] S. Yuasa, T. Nagahama, A. Fukushima, Y. Suzuki, and K. Ando, *Nat. Mater.* **3**, 868 (2004).
- [6] S. S. Parkin, C. Kaiser, A. Panchula, P. M. Rice, B. Hughes, M. Samant, and S.-H. Yang, *Nat. Mater.* **3**, 862 (2004).
- [7] M. Shiga, S. Sakamoto, T. Tsujikawa, R. Ando, K. Amemiya, and S. Miwa, *Phys. Rev. B* **104**, L140406 (2021).
- [8] M. Tsujikawa, S. Haraguchi, and T. Oda, *J. Appl. Phys.* **111**, 083910 (2012).
- [9] K. Nakamura, T. Nomura, A. M. Pradipto, K. Nawa, T. Akiyama, and T. Ito, *J. Magn. Magn. Mater.* **429**, 214 (2017).
- [10] S. Miwa, M. Suzuki, M. Tsujikawa, K. Matsuda, T. Nozaki, K. Tanaka, T. Tsukahara, K. Nawaoka, M. Goto, Y. Kotani, T. Ohkubo, F. Bonell, E. Tamura, K. Hono, T. Nakamura, M. Shirai, S. Yuasa, and Y. Suzuki, *Nat. Commun.* **8**, 15848 (2017).
- [11] T. Nozaki, A. Kozioł-Rachwał, M. Tsujikawa, Y. Shiota, X. Xu, T. Ohkubo, T. Tsukahara, S. Miwa, M. Suzuki, S. Tamaru, H. Kubota, A. Fukushima, K. Hono, M. Shirai, Y. Suzuki, and S. Yuasa, *NPG Asia Mater.* **9**, e451 (2017).
- [12] H. Sukegawa, H. Xiu, T. Ohkubo, T. Furubayashi, T. Niizeki, W. Wang, S. Kasai, S. Mitani, K. Inomata, and K. Hono, *Appl. Phys. Lett.* **96**, 212505 (2010).
- [13] H. Sukegawa, Y. Miura, S. Muramoto, S. Mitani, T. Niizeki, T. Ohkubo, K. Abe, M. Shirai, K. Inomata, and K. Hono, *Phys. Rev. B* **86**, 184401 (2012).
- [14] J. Koo, H. Sukegawa, and S. Mitani, *Phys. Status Solidi RRL* **8**, 841 (2014).
- [15] Q. Xiang, R. Mandal, H. Sukegawa, Y. K. Takahashi, and S. Mitani, *Appl. Phys. Express* **11**, 063008 (2018).
- [16] K. Masuda and Y. Miura, *Phys. Rev. B* **98**, 224421 (2018).
- [17] T. Nozaki, T. Nozaki, T. Yamamoto, M. Konoto, A. Sugihara, K. Yakushiji, H. Kubota, A. Fukushima, and S. Yuasa, *NPG Asia Mater.* **14**, 5 (2022).
- [18] S. Sakamoto, T. Nozaki, S. Yuasa, K. Amemiya, and S. Miwa, *Phys. Rev. B* **106**, 174410 (2022).
- [19] J. Chen, S. Sakamoto, H. Kosaki, and S. Miwa, *Phys. Rev. B* **107**, 094420 (2023).
- [20] M. L. Huggins and J. E. Mayer, *J. Chem. Phys.* **1**, 643 (1933).
- [21] A. Rajanikanth, T. Hauet, F. Montaigne, S. Mangin, and S. Andrieu, *Appl. Phys. Lett.* **103**, 062402 (2013).
- [22] P. B. Johnson and R. W. Christy, *Phys. Rev. B* **9**, 5056 (1974).
- [23] S. Sakamoto, M. Tsujikawa, M. Shirai, K. Amemiya, and S. Miwa, *ACS Appl. Electron. Mater.* **4**, 1794 (2022).
- [24] B. D. Cullity and C. D. Graham, *Introduction to Magnetic Materials* (Wiley, New Jersey, 2011).
- [25] H. J. G. Draaisma and W. J. M. de Jonge, *J. Appl. Phys.* **64**, 3610 (1988).
- [26] T. L. Monchesky and J. Unguris, *Phys. Rev. B* **74**, 241301(R) (2006).
- [27] Th. Mühge, K. Westerholt, H. Zabel, N. N. Garif'yanov, Yu. V. Goryunov, I. A. Garifullin, and G. G. Khaliullin, *Phys. Rev. B* **55**, 8945 (1997).
- [28] E. Kita, M. Ochi, T. Erata, and A. Tasaki, *J. Magn. Magn. Mater.* **117**, 294 (1992).
- [29] Y. Kitaoka and H. Imamura, *J. Magn. Magn. Mater.* **572**, 170596 (2023).
- [30] P. Luches, S. Benedetti, M. Liberati, F. Boscherini, I. I. Pronin, and S. Valeri, *Surf. Sci.* **583**, 191 (2005).